ADVANCED HEALTHCARE MATERIALS
www.advhealthmat.de

A Biodegradable Fiber Calcium Ion Sensor by Covalently Bonding Ionophores on Bioinert Nanoparticles

Sihui Yu, Chengqiang Tang, Sijia Yu, Wenjun Li, Jiajia Wang, Ziwei Liu, Xinheng Yan, Liyuan Wang, Yiqing Yang, Jianyou Feng, Jiaqi Wu, Kailin Zhang, Hang Guan, Yue Liu, Songlin Zhang, Xuemei Sun, and Huisheng Peng*

Implantable sensors, especially ion sensors, facilitate the progress of scientific research and personalized healthcare. However, the permanent retention of implants induces health risks after sensors fulfill their mission of chronic sensing. Biodegradation is highly anticipated; while; biodegradable chemical sensors are rare due to concerns about the leakage of harmful active molecules after degradation, such as ionophores. Here, a novel biodegradable fiber calcium ion sensor is introduced, wherein ionophores are covalently bonded with bioinert nanoparticles to replace the classical ion-selective membrane. The fiber sensor demonstrates comparable sensing performance to classical ion sensors and good flexibility. It can monitor the fluctuations of Ca^{2+} in a 4-day lifespan in vivo and biodegrade in 4 weeks. Benefiting from the stable bonding between ionophores and nanoparticles, the biodegradable sensor exhibits a good biocompatibility after degradation. Moreover, this approach of bonding active molecules on bioinert nanoparticles can serve as an effective methodology for minimizing health concerns about biodegradable chemical sensors.

1. Introduction

Implantable chemical sensors contribute to the advancement of emerging biomedical tools.[1] These tools unveil the occurrence and mechanisms of diseases, providing patients with personalized medical advice. As a crucial subset of implantable chemical sensors, ion sensors play a vital role in predicting various organic and psychological diseases.[2] For instance, the fluctuation of Ca^{2+} is closely associated with diseases such as heart failure, hypertension, depression, and electrolyte imbalance.[3] Miniaturized and flexible chemical sensors have been developed to enable the chronic monitoring of biochemicals in vivo. After the operational lifespan, these sensors are expected to degrade safely to avoid excessive removal operations or health risks associated with the permanent presence of the sensor.[4] However, biodegradable chemical sensors have been rarely reported, in strong contrast to the abundant research on biodegradable sensors for physical signals such as pressure and temperature.[5]

This should be attributed to the unique composition of chemical sensors.[6] Typically, the specific sensing capability of chemical sensors relies on recognition molecules, which are indispensable components but may be toxic.[7] In the case of non-degradable chemical sensors, these molecules are encapsulated by polymers, rendering their toxicity negligible. However, with biodegradable devices, these molecules may move freely within the tissues and organs, potentially causing toxicity. Specifically, ion sensors usually consist of electrodes, a transduction layer, and an ion-selective membrane. The electrodes and transduction layer can be easily replaced by biodegradable materials, except for the ion-selective membrane.[8] As the most crucial component in ion sensors, the ion-selective membrane comprises ionophores, plasticizers, ion exchangers, and a polymer matrix. With the assistance of plasticizers, ionophores and ion exchangers move freely within the polymer matrix, and the target ions are directionally concentrated to change the potential of the membrane.[9] However, it is concerning that the migration and leakage of ionophores, plasticizers, and ion exchangers may lead to biotoxicity in the case of degradation.[7,10] Therefore, developing an effective and biocompatible degradable ion sensor is still challenging.

Here, we introduce a novel biodegradable fiber Ca^{2+} sensor (BFCS). The BFCS is composed of collagen fibers, polypyrrole (PPy), gold nanoparticles (AuNPs), and poly(octanediol citrate) (POC). Crucially, Ca^{2+} ionophores with acetylene-terminated groups are covalently bonded with AuNPs, which replace the function of the classical ion-selective membrane (**Figure 1a**). The BFCS exhibits comparable sensing performance with classical ion sensors and is implanted into a rat to monitor the occurrence of electrolyte imbalance. The good alignment between in

S. Yu, C. Tang, S. Yu, W. Li, J. Wang, Z. Liu, X. Yan, L. Wang, Y. Yang, J. Feng, J. Wu, K. Zhang, H. Guan, Y. Liu, S. Zhang, X. Sun, H. Peng
State Key Laboratory of Molecular Engineering of Polymers
Department of Macromolecular Science
Institute of Fiber Materials and Devices
and Laboratory of Advanced Materials
Fudan University
Shanghai 200438, China
E-mail: sunxm@fudan.edu.cn

The ORCID identification number(s) for the author(s) of this article can be found under https://doi.org/10.1002/adhm.202400675

DOI: 10.1002/adhm.202400675

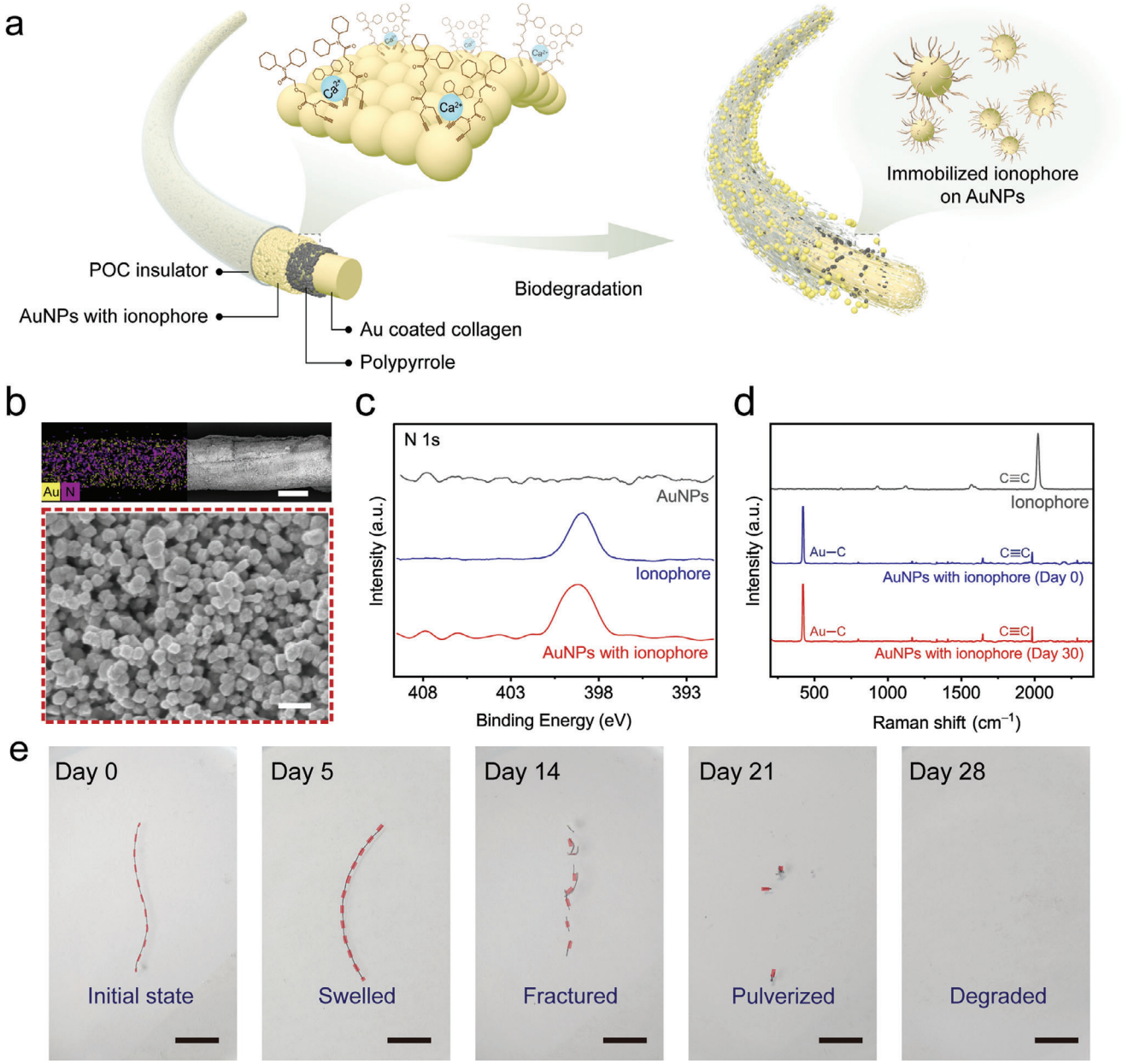

Figure 1. Schematic diagram and the structure of biodegradable fiber calcium ion sensor (BFCS). a) Schematic illustration of the BFCS and its degradation process. POC, poly(octanediol citrate); AuNPs, gold nanoparticles. b) Energy dispersive spectroscopy (EDS) mapping and scanning electron microscopy (SEM) images of the BFCS, showing AuNPs with ionophores on the surface. Scale bars: 50 μm (top) and 200 nm (bottom). c) N 1s X-ray photoelectron spectrometer (XPS) spectra of AuNPs, Ca^{2+} ionophore, and AuNPs with ionophore. d) Raman spectra of Ca^{2+} ionophore, newly prepared AuNPs with ionophore (Day 0), and AuNPs with ionophore after degradation (Day 30). e) Digital photographs of the BFCS during degradation process. The red dashed line highlighted the profile of the residues. Scale bar: 5 mm.

vivo and ex situ data collected with BFCS and Ca^{2+} assay kits demonstrates the reliability of BFCS. The BFCS undergoes the hydration and degradation process within ≈4 weeks. Throughout the whole process, Ca^{2+} ionophores are immobilized stably on AuNPs. Benefiting from this design strategy, BFCS exhibits excellent biocompatibility in both acute and chronic statues, which are inspected, respectively, after implantation and after biodegradation.

2. Results and Discussion

2.1. Designing Strategy and Fabrication of BFCS

The BFCS was fabricated according to the principle of restricting ionophores after biodegradation. First, collagen fiber was chosen as the biodegradable substrate material for its matured and extensive usage in clinical practice.[11] The collagen fiber

was sputtered with Au to establish a conductive substrate, and then, we in situ synthesized PPy as the capacitive layer. The PPy provided a larger capacitance for the sensor, which could effectively enhance the sensitivity of BFCS.[12] AuNPs were further electrodeposited as an anchoring base (Figure 1b; Figures S1–S3, Supporting Information). The size of ≈200 nm could make balance between sensor sensitivity and biocompatibility after the degradation of BFCS (Figure S4, Supporting Information). Subsequently, the pre-synthesized Ca^{2+} ionophores were immobilized on AuNPs through Au—C bonds established between Au and acetylene-terminated groups (Figures S5–S7, Supporting Information). The Au—C bonds exhibited a superior stability and electrochemical performance compared to Au—S bonds in physiological conditions,[13] which was a precious character that could be applied in biodegradable sensors for in vivo applications. The appearance of the N 1s peak in the X-ray photoelectron spectrometer (XPS) spectra and the characteristic peak (432 cm^{-1}) of Au—C bonds in the Raman spectra showed the successful immobilization of Ca^{2+} ionophores (Figure 1c,d; Figure S8, Supporting Information). Finally, the BFCS was insulated by POC as a biodegradable insulator.[14] Thus, the BFCS was fabricated in a diameter of ≈120 µm with electrical insulation properties to offer a better signal-to-noise ratio (Figure S9, Supporting Information).[4c,15]

A series of images exhibited the immersion of BFCS in simulated body fluid to replicate the in vivo degradation process (Figure 1e; Figure S10, Supporting Information). The BFCS swelled in the first 5 days and then lost its shape in 2 weeks. Subsequently, the BFCS fractured and gradually disappeared in ≈4 weeks. The weight variation of residues corresponded with the degradation process. It remained almost the same in the first several days and decreased rapidly in the subsequent periods (Figure S11, Supporting Information). The residues were studied by ultraviolet–visible spectra and dynamic light scattering, confirming that the residues were composed of pulverized PPy and AuNPs, with diameters varying from 100 to 300 nm (Figures S12 and S13, Supporting Information).[16] Raman and infrared spectra confirmed that Ca^{2+} ionophores were stably immobilized on AuNPs after degradation (Figure 1d; Figure S14, Supporting Information), indicating the success of the fabrication approach.[13b,17] In addition, the duration of the biodegradation process could be adjusted by employing alternative degradable substrates, and insulating materials, such as polyglycolide-lactide and polyglycolic acid, could extend the lifespan of the sensor (Table S1, Supporting Information).[18]

2.2. Sensing Performance of BFCS

The sensing performance of BFCS is thoroughly studied to evaluate its reliability. Along with the increase in the concentration of Ca^{2+}, a dynamic balance between the adsorption and desorption of Ca^{2+} exists on AuNPs with Ca^{2+} ionophores. This is attributed to the distinctive molecular structure of the Ca^{2+} ionophore, which is formed by a pair of ester bonds and two hexatomic rings. By assembling three of the Ca^{2+} ionophores, a hole of ≈105 nm can be arranged.[19] Due to ion polarity and volume consistency, Ca^{2+} is selectively concentrated on the surface of BFCS. As positively charged particles, the accumulation of Ca^{2+} elevates the potential of BFCS; while; the potential of the reference electrode remains constant, thereby altering the open-circuit potential in the output of the sensor. The interaction between the ionophore and Ca^{2+} is a reversible dynamic equilibrium process (Figure S15, Supporting Information), ensuring continuous monitoring.

The sensitivity and detection range of BFCS were properly assessed through the linear range (R^2 = 0.998) (**Figure 2**a). The detection limit of the BFCS ranged from 6.92 to 10 mM, covering the fluctuation range in organisms, satisfying the utilization as an implantable biosensor.[20] The sensitivity of BFCS reached 21.65 mV lg^{-1} [Ca^{2+}], comparable to classical implantable calcium ion sensors. Besides, thanks to the strictly controlled manufacturing process, the reproducibility of BFCS was determined as ≈97% (Figure S16, Supporting Information). The reversibility of biosensors was crucial for continuous monitoring, serving as one of the foundations for providing reliable outputs. By increasing and then restoring the concentration of Ca^{2+} step-wise, we demonstrated the BFCS with a comprehensive reversibility of ≈98%. Besides, signals collected from BFCS maintained stable during intervals (Figure 2b). The responding time of BFCS was determined as 1.2 s, which decided the temporal resolution of the sensor (Figure 2c). The satisfying time resolution enabled BFCS to track the fluctuation of Ca^{2+} in real-time and promptly alert the occurrence of diseases. Further, different kinds of interference ions were infused in sequence to estimate the anti-interference capability of BFCS. The BFCS exhibited excellent selectivity toward Ca^{2+}, and relevantly, negligible response to interference ions, including cations and anions (Figure 2d).

Whether the BFCS can withstand the stress or unexpected tension conducted by tissues is an essential factor for the durability of implantable sensors.[21] Hence, the mechanical properties were investigated. Comparing with the national standard of degradable sutures with a breaking force of 1.76 N, the BFCS exhibited a superior performance of 3.90 N (Figure 2e). To simulate various tough mechanical interference with tissues, the BFCS underwent bending, twisting, and friction activities. The sensitivity and impedance magnitude of BFCS changed slightly during those interferences, indicating reliable output performance under vigorous activities (Figure 2f; Figure S17, Supporting Information).

2.3. Sensing and Degradation of BFCS In Vivo

As a proof of working in vivo, the BFCS was implanted into the inferior vena cava of rats with the assistance of an injection syringe. While monitoring the fluctuation of Ca^{2+} in vivo, a certain volume of calcium gluconate saline was injected from the femoral vein to induce an electrolyte disturbance disease (**Figure 3**a). To assess the accuracy of BFCS, we calibrated the concentration of Ca^{2+} ex situ by blood calcium content assay kits. The concentration of Ca^{2+} remained balanced in the first 2000 s before the induction of calcium gluconate saline. The initial Ca^{2+} concentration in the peripheral blood of the rats was ≈1 mM. After the induction of calcium gluconate saline, the in vivo real-time monitoring conducted by BFCS indicated that the Ca^{2+} concentration increased to over 5 mM, consistent with ex situ results from assay kits. Similar results were obtained on the 2nd and 4th day after implantation by the same BFCS. The matching rate between the

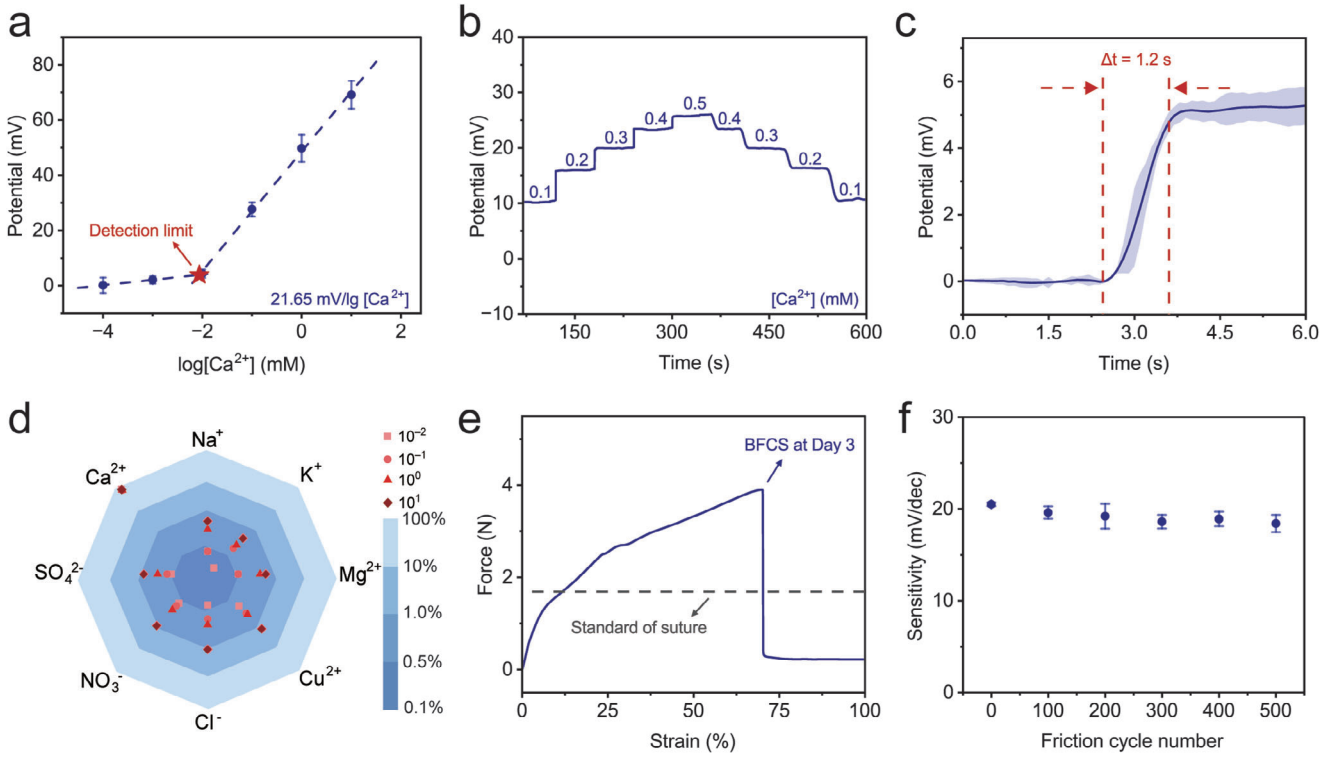

Figure 2. Sensing performance and stability of the BFCS. a) Sensitivity and detection limit of the BFCS. The dashed straight line was fitted from the potential difference response. Error bars, mean ± SD ($n = 3$). The open-circuit potential difference (ΔE, vs Ag/AgCl) was collected by the electrochemical workstation. b) Reversibility of the BFCS by gradually increasing Ca^{2+} concentration from 0.1 to 0.5 mM, and then, restoring. c) The responding time of the BFCS to Ca^{2+} concentration varied from 0.1 to 0.6 mM. The shaded range indicated the mean ± SD, and the solid curve represented the averaged potential signal ($n = 3$). d) Anti-interference performance of the BFCS between Ca^{2+} and other ions in different concentration. Potential changes of BFCS to Ca^{2+} were determined as 100%. e) The mechanical test of BFCS soaked in saline for 3 days compared with the national standard of degradable sutures (grey dashed line). f) The sensitivity of BFCS during 500 friction cycles on tissue substitutes. Error bars showed the mean ± SD ($n = 3$).

BFCS and ex situ results from assay kits was ≈90% in the first 4 days after implantation, which was comparable to other ion sensors (Table S2, Supporting Information).

However, the sensitivity of BFCS notably decreased from ≈21 to ≈15 mV lg^{-1} [Ca^{2+}] with a large standard deviation on the 5th day after implantation, indicating the failure of the sensor (Figure 3b,c; Figure S18, Supporting Information). Thus, the lifespan of the BFCS was confirmed to be 4 days as a precautionary measure.[22] In the first 4 days, the collagen fiber inside BFCS gradually swelled and dilated until cracks emerged on the surface. Subsequently, the sensitivity of BFCS remarkably decreased because the inner PPy layer contacted to the fluid, generating an unauthentic potential draft.[10a,23] 3D reestablished computed X-ray tomography (CT) images provided a direct pathway to follow up the degradation process in vivo (Figure 3d). Initially, the BFCS exhibited stably without noticeable transformation when swelling. After that, the BFCS cracked and broke into large pieces (Week 2), and finally, turned into particles too small to observe under CT (Week 4). The biodegradation process mentioned above aligned properly with the observations in digital photographs (Figure S19, Supporting Information). During the implantation and degradation processes of the BFCS, the body weights of the experimental group and the control group without implants improved slowly with age proportionally, indicating a healthy physical condition (Figure S20, Supporting Information).

2.4. The Biocompatibility of BFCS

The biocompatibility of BFCS was systematically investigated to verify the security in vivo. We chose the 3rd day after implantation as the point in time to investigate the biocompatibility of BFCS in working conditions and the 8th week as the chronic time point because BFCS degraded in about 4 weeks, and small particles were exhaustively invisible in about 8 weeks. Hematoxylin-eosin (H&E) and immunohistochemical staining were used to characterize the cell distribution surrounding BFCS. Specifically, the nuclei, macrophage cells, and neutrophils were stained by 4′,6-diamidino-2-phenylindole (DAPI), adhesion G protein-coupled receptor E1 (F4/80), and proliferation marker protein Ki-67 (LY-6G), respectively. Compared with the control group; although, acute immune responses were observed on the 3rd day due to the auxiliary implantation by syringe, no macrophage aggregation or inflammation occurred on the 8th week after implantation when the BFCS was thoroughly degraded.[21] Statistics of fluorescence further confirmed the biocompatibility of the sensor (**Figure 4a**; Figure S21, Supporting Information). Moreover, H&E staining of major internal organs including the heart, liver, spleen, lung, and kidney was analyzed, and no significant pathological changes occurred (Figure 4b). The complete blood counts and blood chemistry tests revealed a benign blood physiology and good holistic health (Figure 4c,d; Figure S22, Supporting Information).

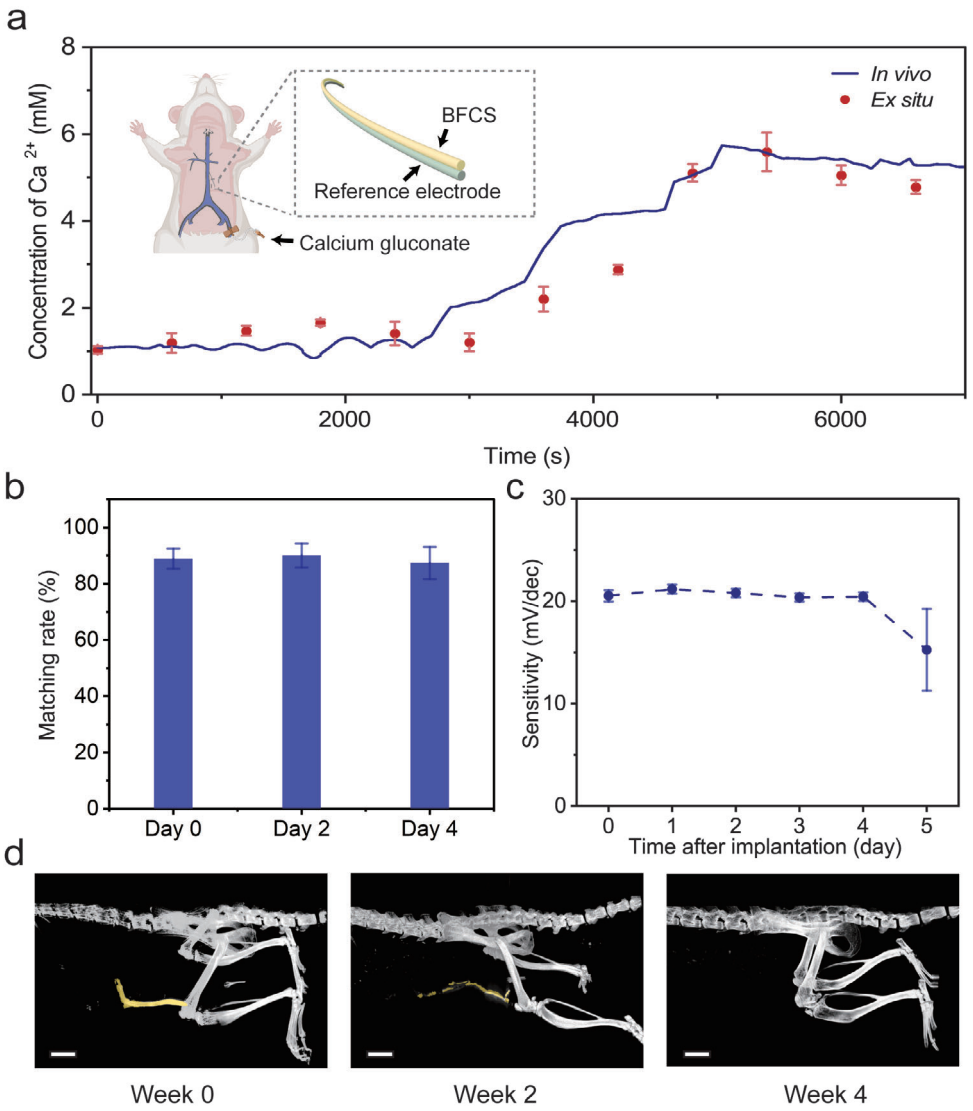

Figure 3. In vivo sensing and biodegradation process of the BFCS. a) The real time monitoring of Ca^{2+} concentration by the BFCS in vivo compared with the ex situ results measured every 10 min. The inserted schematic diagram indicated that the BFCS and the reference electrode were parallelly assembled and implanted into the inferior vena cava, and calcium gluconate saline solution was injected through the femoral vein. The red dots with error bars indicated the mean ± SD of ex situ assay kits results ($n = 3$). b) The matching rate between in vivo and ex situ results. The matching of in vivo and ex situ results approved the reliability of BFCS. Error bars, mean ± SD, $n = 3$. c) The changes of sensitivity over time after implantation, and the lifespan of BFCS was determined as 4 days. Error bars, mean ± SD, $n = 5$. d) 3D reestablished computed X-ray tomography (CT) images of mice implanted with BFCS, which gradually disappeared in about 4 weeks. The yellow shaded range highlighted the profile of the residues of the BFCS. Scale bar: 5 mm.

The satisfying results of biocompatibility demonstrated that the strategy of immobilizing active molecules on bioinert materials to fabricate biodegradable implantable chemical sensors was an effective approach to enhance the biocompatibility after degradation.

3. Conclusion

In this study, we proposed a new design strategy for biodegradable chemical sensors and introduced a biodegradable fiber calcium ion sensor. Immobilized ionophores with bioinert nanoparticles were utilized to replace classical ion-selective membranes, minimizing health risks after biodegradation. The BFCS exhibited stable sensitivity within a controllable lifespan of 4 days and degraded within 4 weeks. BFCS outputs in in vivo and ex situ calibrations demonstrated excellent consistency throughout the lifespan, whose performance was comparable with classical ion-selective sensors. Further, throughout the entire lifespan of BFCS, from implantation to biodegradation, ionophores were consistently immobilized on bioinert nanoparticles, minimizing the leakage into the organism. Finally, the strategy of immobilizing active molecules we proposed here may contribute to the evolution of various biodegradable chemical sensors.

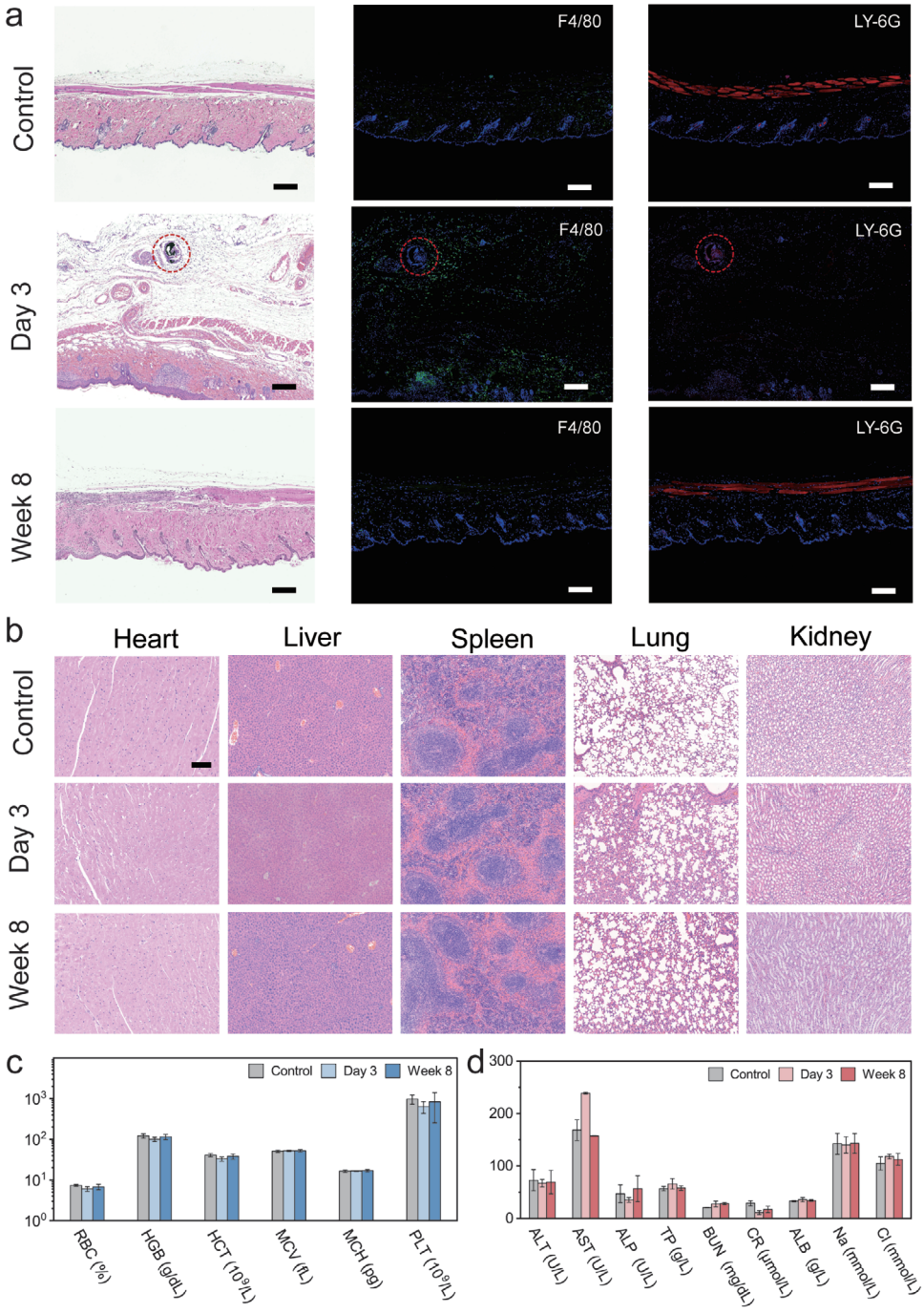

Figure 4. Biocompatibility of the BFCS. a) Hematoxylin-eosin (H&E) and immunohistochemical staining images of subcutaneous tissues taken on the 3rd day and the 8th week after implantation. Blue, green, and red colors corresponded to DAPI (the marker of nuclei), F4/80 (the marker of macrophage cells), and LY-6G (the marker of neutrophils), respectively. Dashed circles indicated the position of BFCS implantation. Scale bars, 200 μm. Biologically independent animals, $n = 3$. b) H&E staining images of internal organs taken on the 3rd day and the 8th week after implantation. Scale bars: 200 μm. Biologically independent animals, $n = 3$. c,d) Analysis of the complete blood counts and blood chemistry tests, revealing the overall health condition, especially blood physiology. RBC, number of red cells; HGB, hemoglobin; HCT, hematocrit value; MCV, mean corpuscular volume; MCH, mean erythrocyte hemoglobin content; PLT, platelet count; ALT, alanine aminotransferase; AST, aspartate transaminase; ALP, alkaline phosphatase; TP, total protein; BUN, blood urea nitrogen; CR, creatinine; ALB, albumin; Na, sodium; Cl, chlorine. Error bars, biologically independent animals, mean ± SD, $n = 3$.

4. Experimental Section

Materials: Collagen fiber (Bangda 7–0) was purchased from Boda medical supplies Co., Ltd. Dicyclohexylamine, chloroauric acid hydrate ($AuClO_4 \cdot 3H_2O$), and *N*-(3-dimethylaminopropyl)-*N'*-ethylcarbodiimide hydrochloride (EDCI) were purchased from Admas Co., Ltd. Diglycolic anhydride was purchased from Alfa Aesar. 1-Hydroxybenzotriazole (HOBT) and calcium gluconate were purchased from Aladdin Scientific Inc. Dipropargylamine was purchased from Leyan Co., Ltd. Pyrrole was purchased from TCI (Shanghai) Development Co., Ltd. All other common reagents were purchased from Greagent Chemical Co., Ltd.

Synthesis of the Ca^{2+} Ionophore: The Ca^{2+} ionophore was synthesized based on the previous report.[3a] Specifically, a mixture of diglycolic anhydride (4.64 g, 40 mmol) and dicyclohexylamine (3.97 mL, 20 mmol) was stirred in dichloromethane at 25 °C for 8 h. Then, the solution was washed with water (w/w) at least three times, and then, with saturated salt solution. Afterward, water was removed with anhydrous Na_2SO_4, and excessive dichloromethane was eliminated through rotary evaporation. This process yielded Compound 1 at 89.42%. Next, Compound 1 (4.41 g, 15 mmol) was dissolved in 100 mL dichloromethane; after that, EDCI (5.73 g, 30 mmol) was added under an ice bath. Once EDCI dissolved, HOBT (4.05 g, 30 mmol) and dipropargylamine (1.40 g, 15 mmol) were introduced into the flask and stirred at 30 °C for 8 h. The resulting mixture was washed with water (w/w) three times, and then, with saturated salt solution (w/w) two times. Water was removed with anhydrous Na_2SO_4, and excessive dichloromethane was evaporated. Finally, the product underwent purification through recrystallization using water and ethanol, yielding 80.39%.

^{1}H NMR of the Ca^{2+} ionophore. ^{1}H NMR (400 MHz, $CDCl_3$, ppm): δ 4.36 (s, 2H), 4.28 (d, $J = 6.5$ Hz, 2H), 4.18 (s, 2H), 3.26 (t, $J = 11.3$ Hz, 1H), 2.90 (s, 1H), 2.40 (s, 2H), 2.27 (s, 1H), 2.21 (s, 1H), 1.76 (d, $J = 13.3$ Hz, 4H), and 1.78–1.03 (m, 18H) (Figure S3, Supporting Information).

^{13}C NMR of the Ca^{2+} ionophore. ^{13}C NMR (400 MHz, $CDCl_3$, ppm): δ 168.59, 167.43, 77.79, 77.64, 73.18, 72.59, 70.41, 69.61, 56.76, 56.07, 35.43, 33.98, 31.24, 29.93, 26.58, 25.82, 25.34, and 25.21 (Figure S4, Supporting Information).

Fabrication of the Biodegradable Fiber Calcium Ion Sensor (BFCS): An 80 nm thick gold layer was initially deposited on the collagen fiber with magnetron sputtering. Subsequently, a pyrrole solution (0.17 M, 10 mL) and KNO_3 solution (0.17 M, 10 mL) were prepared. The Au/collagen fiber was immersed in a mixed solution with pyrrole and KNO_3 in 1:1 ratio, followed by soaking in deionized water for 1 h to infiltrate thoroughly. Next, 5 mL $FeCl_3 \cdot 6H_2O$ solution (0.23 M) was slowly added dropwise into the pyrrole solution under an ice bath. The solution was gently shaken for 1.5 h and kept in an ice bath to slow the reaction rate, resulting in fibers loaded with polypyrrole (PPy). Then, the as-prepared collagen fiber/Au/PPy was removed from the reaction solution and soaked overnight in deionized water to eliminate excessive $FeCl_3$. Afterward, the fibers were activated by soaking in 0.1 M HCl for 10 min prior to the electrodeposition of gold nanoparticles. Subsequently, the as-prepared fiber was immersed in an electrolytic tank containing 1.5 mM $HAuCl_4$. By carrying out the chronoamperometry method, the as-prepared fiber was applied with a potential of −0.2 V versus Ag/AgCl for 6 s to obtain AuNPs on the fiber. Finally, the fiber was immersed in an ethanol solution of the Ca^{2+} ionophore (0.2 mM) under a deoxygenated environment for 12 h at 60 °C, and then, dried for 24 h at room temperature to obtain the BFCS.

Preparation of Ag/AgCl Reference Electrode: PVB (395.5 mg) was dissolved in methanol (5 mL) to obtain a PVB solution. After ultrasonic dispersion for 30 min, NaCl (250 mg) and $AgNO_3$ (250 mg) were added to the as-prepared solution. Subsequent to vigorous shaking for 30 min, the mixture was exposed to light for 3 h to obtain a light purple suspension. Finally, a layer of PVB suspension was coated onto the Au/collagen fiber and dried overnight to obtain the reference electrode.

Insulation of the Electrodes: Poly(octanediol citrate) (POC) was synthesized as previously reported.[14a] The pre-polymer solution was coated on the electrodes and crosslinked at 100 °C at oxygen-free atmosphere for 1 day. The effect of insulation was verified by impedance test conducted at 1000 Hz.

Characterization: Photographs were taken with a digital camera (SONY A6000, Japan). Optical microscopy images were taken by Olympus EX51. Zeiss Gemini SEM500 FESEM was used to obtain the scanning electron microscopy (SEM) images. X-ray photoelectron spectroscopy (XPS) was acquired by a scanning XPS Microprobe (Thermo Scientific K-Alpha$^+$) using a micro-focused monochromator Al K-alpha X-ray source. Raman spectroscopy was performed using Renishaw InVia Qontor equipped with an Ar ion laser with 738 nm excitation wavelength at 25% laser power. ^{1}H and ^{13}C nuclear magnetic resonance (NMR) spectra were obtained using a Bruker AVANCE III HD spectrometer (400 M). Matrix-assisted laser desorption/ionization time-of-flight mass spectrometry (MALDI-TOF MS) was measured by using an AB SCIEX 5800 mass spectrometer, with trans-2-[3-(4-tert-Butylphenyl)−2-methyl-2-propenylidene]-malononitrile as the matrix and sodium trifluoroacetate as the ionization reagent. Absorption spectra were recorded using an ultraviolet–visible spectrophotometer (Perkin–Elmer Lambda 750) in the wavelength of 300–800 nm. The electrochemical deposition and characterizations were characterized by the CHI660e electrochemical workstation (Shanghai Chenhua Co., Ltd). Electrochemical impedance spectroscopy was obtained using A.C. impedance parameters within a frequency range from 10^1 to 10^5 Hz. The broken force of the sensor was tested by a table-top universal testing instrument (Zhongchen Inc, resolution ~ μN). The fiber was placed with a compression clamp and stretched with a velocity of 10 mm s^{-1}. The tissue section fluorescence images were obtained and analyzed through Nikon Eclipse C1 and Pannoramic MIDI.

Implantation of the BFCS: The animal experimental protocols were approved by the Animal Experimentation Committee of Fudan University (certificate number: SYXK2020-0032). All animals were treated following the guidelines for the care and usage of experimental animals outlined by the National Institutes of Health and Fudan University. Male rats (CD-SD, 9 weeks old, Charles River Laboratories Co., Ltd.) were housed under controlled temperature and humidity conditions with access to abundant food and water. The rats were anesthetized with 1.5% isoflurane mixed with air and secured in a stereotactic frame. Subsequently, the fur was shaved, and the skin was thoroughly disinfected with iodophor. After exposing the inferior vena cava, a biodegradable fiber calcium ion sensor (BFCS) was injected into the inferior vena cava with the assistance of a syringe needle. The BFCS was then secured with a small amount of tissue adhesive (3 M Co., Ltd) and connected to epidermal sites through lead wires.

Ex Situ Calibration of the BFCS: Prior to the implantation of BFCS, the BFCS ex situ was calibrated. Specifically, the potential of BFCS in calcium chloride solutions of 0.01, 0.1, and 1 mM was recorded to calculate the sensitivity of the sensor. To validate the reliability of BFCS, the potential was matched with the ex situ test results conducted by assay kits at 1 min after starting the test.

In Vivo Monitoring the Concentration of Ca^{2+}: The rats were assessed for an electrolyte imbalance disease on the 1st, 2nd, and 4th days after implantation. Anesthesia was induced by 1.5% isoflurane mixed with air, and the rats were secured in a stereotactic frame. The BFCS and the reference electrode were connected to the electrochemical workshop CHI660e. The open-circuit potential between BFCS and the reference electrode was continuously recorded. After 20 min, a solution of 5% calcium gluconate (0.7 mL) was injected into the femoral vein to induce a rapid elevation of blood calcium concentration in rats; thus, creating a model of electrolyte disorder. Fluctuations in calcium ion concentration were continuously recorded for at least 2 h.

Ex Situ Calibrating the Concentration of Ca^{2+}: Rats were subjected to model electrolyte disorder disease. The rats were anesthetized with 1.5% isoflurane mixed with air and secured in a stereotactic frame. Subsequently, the fur was shaved, and the skin was thoroughly disinfected with iodophor. After exposing the inferior vena cava and the femoral vein, 150 μL of blood was initially drawn from the inferior vena cava as a reference sample. Then, an aqueous solution of 5% calcium gluconate (0.7 mL) was injected into the femoral vein to raise the calcium ion concentration within the rat. After injection, 150 μL blood samples were collected from the inferior vena cava at a 10-min interval over the 2-h experimental period, with careful monitoring of vital signs. Following the coagulation of blood samples, blood clots were centrifuged at 3000 rpm for 10 min to obtain

serum. According to the principle that a certain amount of red complex can be generated from the reaction between free calcium ions and GBHA, the calcium concentration in blood was determined by using a blood calcium content assay kit (Boxbio Science & Technology Co. Ltd) and measured with a microplate reader ($n = 3$).

Hematoxylin-Eosin (H&E) Staining and Immunohistochemistry Test: After euthanizing the animals, relevant tissues were extracted and preserved in a 4% paraformaldehyde aqueous solution. Tissues were dehydrated using the graded ethanol dehydration method and embedded in paraffin blocks. Subsequently, paraffin was sectioned into slices of 5 µm thickness and stored at room temperature. For H&E staining, the sections were sequentially treated with xylene, anhydrous ethanol, 75% ethanol, and water. They were then immersed successively in differentiation solution, reblue solution, and hematoxylin staining solution for 5 min each. Afterward, the sections were dehydrated, followed by a 5-min immersion in an eosin staining solution to complete the eosin staining. The sections were rinsed with distilled water before each solution change. Before immunofluorescence staining, antigen retrieval was performed on the sections using citrate buffer, followed by a 30-min incubation in a BSA solution. For the immunofluorescence staining, 4′6-diamidino-2-phenylindole (DAPI, G1012, Servicebio) was implemented to stain the nuclei of all cells. The primary antibodies were the adhesion G protein-coupled receptor E1 (F4/80, G11027, Servicebio) and proliferation marker protein Ki-67 (LY-6G, G111499, Servicebio). HRP conjugated goat anti-rabbit IgG (H+L) (1:500, GB23303, Servicebio) and Cy3 conjugated goat anti-rabbit IgG (H+L) (1:400, GB21303, Servicebio) were used as the secondary antibodies.

Statistical Analysis: The statistical analysis was conducted with Origin, Image J, and Excel. The results are presented as the mean ± SD. The statistical tests, replicate number, error bars, and *P*-values are indicated in the figure legends.

Supporting Information

Supporting Information is available from the Wiley Online Library or from the author.

Acknowledgements

The authors thank Hexige Saiyin of Fudan University for helpful discussions about the biocompatibility of the BFCS. This work was supported by NSFC (52122310, 22075050, T2321003, 22335003) and MOST (2022YFA1203001, 2022YFA1203002).

Conflict of Interest

The authors declare no conflict of interest.

Data Availability Statement

The data that support the findings of this study are available in the Supporting Information of this article.

Keywords

biodegradable, biosensors, fiber, flexible electronics, ionophores

Received: February 22, 2024
Revised: May 21, 2024
Published online: June 11, 2024

[1] a) Y. Luo, M. Abidian, J. Ahn, D. Akinwande, A. Andrews, M. Antonietti, Z. Bao, M. Berggren, C. Berkey, C. Bettinger, J. Chen, P. Chen, W. Cheng, X. Cheng, S. Choi, A. Chortos, C. Dagdeviren, R. Dauskardt, C. Di, M. Dickey, X. Duan, A. Facchetti, Z. Fan, Y. Fang, J. Feng, X. Feng, H. Gao, W. Gao, X. Gong, C. Guo, et al., *ACS Nano* **2023**, *17*, 5211; b) L. Wang, S. Xie, Z. Wang, F. Liu, Y. Yang, C. Tang, X. Wu, P. Liu, Y. Li, H. Saiyin, S. Zheng, X. Sun, F. Xu, H. Yu, H. Peng, *Nat. Biomed. Eng.* **2020**, *4*, 159.

[2] Y. Liu, Z. Liu, Y. Zhou, Y. Tian, *JACS Au* **2023**, *3*, 1572.

[3] a) Y. Liu, Z. Liu, F. Zhao, Y. Tian, *Angew. Chem., Int. Ed.* **2021**, *60*, 14429; b) J. Wang, L. Wang, Y. Yang, H. Li, X. Huang, Z. Liu, S. Yu, C. Tang, J. Chen, X. Shi, W. Li, P. Chen, Q. Tong, H. Yu, X. Sun, H. Peng, *Adv. Mater.* **2024**, *36*, 2309862; c) H. Yang, Z. Qian, J. Wang, J. Feng, C. Tang, L. Wang, Y. Guo, Z. Liu, Y. Yang, K. Zhang, P. Chen, X. Sun, H. Peng, *Adv. Funct. Mater.* **2022**, *32*, 2204794.

[4] a) Y. Zhang, G. Lee, S. Li, Z. Hu, K. Zhao, J. Rogers, *Chem. Rev.* **2023**, *123*, 11722; b) M. Lin, H. Hu, S. Zhou, S. Xu, *Nat. Rev. Mater.* **2022**, *7*, 850; c) L. Wu, X. Shi, Z. Wu, *Adv. Funct. Mater.* **2023**, *33*, 2211454; d) T. Mei, C. Wang, M. Liao, J. Li, L. Wang, C. Tang, X. Sun, B. Wang, H. Peng, *J. Mater. Chem. A* **2021**, *9*, 10104.

[5] a) J. Qin, L. Yin, Y. Hao, S. Zhong, D. Zhang, K. Bi, Y. Zhang, Y. Zhao, Z. Dang, *Adv. Mater.* **2021**, *33*, 2008267; b) J. Reeder, Z. Xie, Q. Yang, M. Seo, Y. Yan, Y. Deng, K. Jinkins, S. Krishnan, C. Liu, S. McKay, E. Patnaude, A. Johnson, Z. Zhao, M. Kim, Y. Xu, I. Huang, R. Avila, C. Felicelli, E. Ray, X. Guo, W. Ray, Y. Huang, M. MacEwan, J. Rogers, *Science* **2022**, *377*, 109; c) Y. Choi, H. Jeong, R. Yin, R. Avila, A. Pfenniger, J. Yoo, J. Lee, A. Tzavelis, Y. Lee, S. Chen, H. Knight, S. Kim, H. Ahn, G. Wickerson, A. Vazquez-Guardado, E. Higbee-Dempsey, B. Russo, M. Napolitano, T. Holleran, L. Razzak, A. Miniovich, G. Lee, B. Geist, B. Kim, S. Han, J. Brennan, K. Aras, S. Kwak, J. Kim, E. Waters, et al., *Science* **2022**, *376*, 1006; d) C. Boutry, Y. Kaizawa, B. Schroeder, A. Chortos, A. Legrand, Z. Wang, J. Chang, P. Fox, Z. Bao, *Nat. Electron.* **2018**, *1*, 314; e) J. Shin, Y. Yan, W. Bai, Y. Xue, P. Gamble, L. Tian, I. Kandela, C. Haney, W. Spees, Y. Lee, M. Choi, J. Ko, H. Ryu, J. Chang, M. Pezhouh, S. Kang, S. Won, K. Yu, J. Zhao, Y. Lee, M. MacEwan, S. Song, Y. Huang, W. Ray, J. Rogers, *Nat. Biomed. Eng.* **2019**, *3*, 37.

[6] a) M. Sorvin, S. Belyakova, I. Stoikov, R. Shamagsumova, G. Evtugyn, *Front. Chem.* **2018**, *6*, 134; b) J. Li, J. Liu, Z. Wu, X. Shang, Y. Li, W. Huo, X. Huang, *Sci. Adv.* **2023**, *9*, eadi3839; c) N. Abramova, J. Moral-Vico, J. Soley, C. Ocana, A. Bratov, *Anal. Chim. Acta* **2016**, *943*, 50; d) J. Hu, W. Zhao, P. Bühlmann, A. Stein, *ACS Appl. Nano Mater* **2017**, *1*, 293.

[7] R. Canovas, S. Sanchez, M. Parrilla, M. Cuartero, G. Crespo, *ACS Sens.* **2019**, *4*, 2524.

[8] H. Wang, S. Zhang, R. Liu, Y. Yin, H. Zeng, G. Ren, M. Zhang, *Anal. Chem.* **2023**, *95*, 8586.

[9] a) E. Zdrachek, E. Bakker, *Anal. Chem.* **2019**, *91*, 2; b) Y. Shao, Y. Ying, J. Ping, *Chem. Soc. Rev.* **2020**, *49*, 4405.

[10] a) K. Maksymiuk, E. Stelmach, A. Michalska, *Membranes* **2020**, *10*, 266; b) P. Melamed, Z. Yaron, *Gen. Comp. Endocrinol.* **1999**, *114*, 19.

[11] a) G. Balakrishnan, J. Song, C. Mou, C. Bettinger, *Adv. Mater.* **2022**, *34*, 2106787; b) R. Feiner, T. Dvir, *Nat. Rev. Mater.* **2017**, *3*, 17076.

[12] a) B. Guo, P. Ma, *Biomacromolecules* **2018**, *19*, 1764; b) A. Ramanaviciene, A. Kausaite, S. Tautkus, A. Ramanavicius, *J. Pharm. Pharmacol.* **2007**, *59*, 311; c) X. Wang, X. Gu, C. Yuan, S. Chen, P. Zhang, T. Zhang, J. Yao, F. Chen, G. Chen, *J. Biomed. Mater. Res., Part A* **2004**, *68A*, 411; d) Z. Zha, X. Yue, Q. Ren, Z. Dai, *Adv. Mater.* **2013**, *25*, 777.

[13] a) R. Weston, Y. Chen, T. Dzwonczyk, J. Veras, A. Sevigny, E. Landis, *J. Phys. Chem. C* **2022**, *126*, 9673; b) C. Zhang, Z. Liu, L. Zhang, A. Zhu, F. Liao, J. Wan, J. Zhou, Y. Tian, *Angew. Chem., Int. Ed.* **2020**, *59*, 20499.

[14] a) J. Yang, A. Webb, G. Ameer, *Adv. Mater.* **2004**, *16*, 511; b) L. Wan, L. Lu, T. Zhu, Z. Liu, R. Du, Q. Luo, Q. Xu, Q. Zhang, X. Jia, *Biomacromolecules* **2022**, *23*, 4268.
[15] M. Sang, K. Kim, J. Shin, K. J. Yu, *Adv. Sci.* **2022**, *9*, e2202980.
[16] a) C. Hong, X. Zhang, C. Wu, Q. Chen, H. Yang, D. Yang, Z. Huang, R. Cai, W. Tan, *ACS Appl. Mater. Interfaces* **2020**, *12*, 54426; b) W. Tian, Y. Li, J. Zhou, T. Wang, R. Zhang, J. Cao, M. Luo, N. Li, N. Zhang, H. Gong, J. Zhang, L. Xie, B. Kong, *ACS Appl. Mater. Interfaces* **2021**, *13*, 8285.
[17] J. Xu, M. Yu, C. Peng, P. Carter, J. Tian, X. Ning, Q. Zhou, Q. Tu, G. Zhang, A. Dao, X. Jiang, P. Kapur, J. Hsieh, X. Zhao, P. Liu, J. Zheng, *Angew. Chem., Int. Ed.* **2018**, *57*, 266.
[18] a) R. Pal, A. Farghaly, C. Wang, M. Collinson, S. Kundu, V. Yadavalli, *Biosens. Bioelectron.* **2016**, *81*, 294; b) C. Boutry, L. Beker, Y. Kaizawa, C. Vassos, H. Tran, A. Hinckley, R. Pfattner, S. Niu, J. Li, J. Claverie, Z. Wang, J. Chang, P. Fox, Z. Bao, *Nat. Biomed. Eng.* **2019**, *3*, 47.
[19] a) M. Huang, X. Li, *Prog. Mater. Sci.* **2022**, *125*, 100885; b) Y. Qin, S. Peper, A. Radu, A. Ceresa, E. Bakker, *Anal. Chem.* **2003**, *75*, 3038.
[20] J. Blaine, M. Chonchol, M. Levi, *Clin. J. Am. Soc. Nephrol.* **2015**, *10*, 1257.
[21] D. Zhang, Q. Chen, C. Shi, M. Chen, K. Ma, J. Wan, R. Liu, *Adv. Funct. Mater.* **2020**, *31*, 2007226.
[22] a) M. Guzinski, J. Jarvis, P. D'Orazio, A. Izadyar, B. Pendley, E. Lindner, *Anal. Chem.* **2017**, *89*, 8468; b) J. Veder, K. Patel, M. Sohail, S. Jiang, M. James, R. Marco, *Electroanalysis* **2012**, *24*, 140; c) V. Krikstolaityte, R. Ding, T. Ruzgas, S. Bjorklund, G. Lisak, *Anal. Chim. Acta* **2020**, *1128*, 19.
[23] C. Rousseau, P. Bühlmann, *Anal. Chem.* **2021**, *140*, 116277.